J. Fluid Mech. (1995), *vol.* 305, *pp.* 111–126

Liquid-metal flow in an insulated rectangular expansion with a strong transverse magnetic field

By JOHN S. WALKER[1] AND BASIL F. PICOLOGLOU[2]

[1] Department of Mechanical and Industrial Engineering, University of Illinois, Urbana, IL 61801, USA

[2] Technology Development Division, Argonne National Laboratory, Argonne, IL 60439, USA

(Received 13 December 1994 and in revised form 25 July 1995)

This paper concerns a steady liquid-metal flow through an expansion or contraction with electrically insulated walls, with rectangular cross-sections and with a uniform, transverse, externally applied magnetic field. One pair of duct walls is parallel to the applied magnetic field, and the other pair diverges or converges symmetrically about a plane which is perpendicular to the field. The magnetic field is assumed to be sufficiently strong that inertial effects can be neglected and that the well-known Hartmann-layer solution is valid for the boundary layers on the walls which are not parallel to the magnetic field. A general treatment of three-dimensional flows in constant-area ducts is presented. An error in the solution of Walker *et al.* (1972) is corrected. A smooth expansion between two different constant-area ducts is treated. In the expansion the flow is concentrated inside the boundary layers on the sides which are parallel to the magnetic field, while the flow at the centre of the duct is very small and may be negative for a large expansion slope. In each constant-area duct, the flow evolves from a concentration near the sides at the junction with the expansion to the appropriate fully developed flow far upstream or downstream of the expansion. The pressure drop associated with the three-dimensional flow increases as the slope increases.

1. Introduction

Liquid-metal flows in electrically insulated ducts with strong magnetic fields occur in many energy conversion and materials processing applications. One example is the use of liquid lithium to extract energy from a fusion reactor and to breed the tritium to fuel the fusing plasma. The liquid lithium must be pumped through the strong magnetic field needed to confine the plasma. For many years, fusion-reactor feasibility studies assumed that no electrically insulating materials could be compatible with hot liquid lithium, so pressure drops were minimized by making the metal duct walls as thin as possible. Recent advances in material science indicate that certain electrically insulating coatings are compatible with hot liquid lithium, so that designs now assume that the duct walls are insulated.

Fully developed flows in constant-area ducts require relatively small pressure gradients because all electric current must flow through the very thin Hartmann layers. The large electrical resistance of these thin layers limits the electric current and the associated electromagnetic (EM) body force opposing the flow. However, at an expansion or contraction or a change in magnetic field strength, axial voltage differences drive circulations of electric current in planes which are perpendicular to the magnetic field. These three-dimensional electric current circulations do not pass

through the Hartmann layers, so they can produce EM body forces opposing the flow which are much larger than those for fully developed flow. These three-dimensional pressure drops may dramatically increase the overall pressure drop needed to drive a given flow rate through a fusion-reactor 'blanket'. In addition to the extra pressure drops, the three-dimensional flow pattern is very important because convective heat transfer plays a key role in determining the thermal performance of the reactor. An expansion or contraction with a uniform transverse magnetic field represents an ideal prototype for investigating the physical phenomena associated with three-dimensional magnetohydrodynamic flows in insulated ducts.

2. Problem formulation

This paper concerns a steady liquid-metal flow through an expansion or contraction with electrically insulated walls, with rectangular cross-sections and with a uniform applied magnetic field. The planar sidewalls are parallel to the applied magnetic field and to each other. The characteristic length L is half the distance between the sides. The top and bottom walls diverge or converge symmetrically about a plane which is perpendicular to the applied magnetic field.

In addition to the externally applied magnetic field, the electric currents in the liquid metal produce a secondary or induced magnetic field. The characteristic ratio of the induced to applied magnetic field strengths is the magnetic Reynolds number, $R_m = \mu_p \sigma U L$. Here μ_p and σ are the magnetic permeability and electrical conductivity of the liquid metal, while U is the characteristic velocity. We assume that R_m is sufficiently small that the induced magnetic field can be neglected. Walker, Ludford & Hunt (1972) showed that the dimensionless electric current density is $O(Ha^{-1/2})$, where $Ha = BL(\sigma/\mu)^{1/2}$ is the Hartmann number, B is the magnetic flux density of the externally applied magnetic field and μ is the viscosity of the liquid metal. Therefore the inductionless assumption requires that $R_m Ha^{-1/2} \ll 1$.

In the Navier–Stokes equation, the characteristic ratio of the EM body-force term to the inertial term is the interaction parameter, $N = \sigma B^2 L/\rho U$, where ρ is the density of the liquid metal. We assume that N is sufficiently large that the inertial term can be neglected everywhere. Walker *et al.* (1972) showed that there are $O(Ha^{1/2})$ dimensionless velocities in sidewall boundary layers with $O(Ha^{-1/2})$ dimensionless thickness and that neglect of inertial effects in these high-velocity-side layers requires $NHa^{-3/2} \gg 1$.

For the dimensionless Cartesian coordinates, the x-axis lies along the centreline of the duct and the y-axis is parallel to the applied magnetic field. The sides are at $z = \pm 1$, the top and bottom are at $y = \pm f(x)$ and the dimensionless applied magnetic field is $\hat{\boldsymbol{y}}$, where $\hat{\boldsymbol{x}}$, $\hat{\boldsymbol{y}}$, $\hat{\boldsymbol{z}}$ are unit vectors. The velocity $\boldsymbol{v}$, pressure p, electric current density $\boldsymbol{j}$ and electric potential function ϕ are normalized by U, σUB^2L, σUB and UBL, respectively. The dimensionless governing equations are

$$0 = -\nabla p + \boldsymbol{j} \times \hat{\boldsymbol{y}} + Ha^{-2} \nabla^2 \boldsymbol{v}, \quad \nabla \cdot \boldsymbol{v} = 0, \tag{1a, b}$$

$$\boldsymbol{j} = -\nabla \phi + \boldsymbol{v} \times \hat{\boldsymbol{y}}, \quad \nabla \cdot \boldsymbol{j} = 0, \tag{1c, d}$$

where (1 *a*) is the inertialess Navier–Stokes equation with the EM body force $\boldsymbol{j} \times \hat{\boldsymbol{y}}$, (1 c) is Ohm's law with the static electric field $-\nabla\phi$ and the induced electric field $\boldsymbol{v} \times \hat{\boldsymbol{y}}$, and (1 *b*, *d*) guarantee conservation of mass and electric charge (Moreau 1990).

The boundary conditions are

$$\boldsymbol{v} = 0, \quad \boldsymbol{j} \cdot \hat{\boldsymbol{n}} = 0 \quad \text{at} \quad y = \pm f(x), \tag{2a, b}$$

$$\boldsymbol{v} = 0, \quad j_z = 0 \quad \text{at} \quad z = \pm 1, \tag{2c, d}$$

where $\hat{\boldsymbol{n}}$ is a unit normal to the top or bottom. Symmetry reduces the domain to $0 \leqslant y \leqslant f(x), 0 \leqslant z \leqslant 1$ with appropriate symmetry conditions, i.e. p is an even function of both y and z, while ϕ is an even function of y and an odd function of z. With the mean dimensional axial velocity at a square cross-section for U, the dimensionless axial velocity must satisfy

$$\int_0^{f(x)} \int_0^1 u(x, y, z)\, \mathrm{d}z\, \mathrm{d}y = 1, \tag{3}$$

where $\boldsymbol{v} = u\hat{\boldsymbol{x}} + v\hat{\boldsymbol{y}} + w\hat{\boldsymbol{z}}$. The solution of the homogeneous linear boundary value problem (1), (2) is scaled by (3). Since the problem is linear, the solution for any contraction is obtained by changing the signs of all variables in the solution for the geometrically similar expansion, i.e. replace the right-hand side of (3) by -1.

Walker *et al.* (1972) presented a large-Hartmann-number asymptotic solution of (1)–(3) with $f(x) = a$, for $-\infty < x \leqslant 0$, and $f(x) = a + bx$, for $0 \leqslant x < \infty$, i.e. for a constant-area duct joined to a semi-infinite expansion with straight diverging top and bottom. In each x = constant cross-section for $y > 0$ and $z > 0$, the domain is divided into (*a*) an inviscid core region with all $O(1)$ derivatives, (*b*) a Hartmann layer with an $O(Ha^{-1})$ thickness between the core and the top at $y = f$, (*c*) a side layer with an $O(Ha^{-1/2})$ thickness between the core and the side at $z = 1$, (*d*) an intersection region with $\Delta y = O(Ha^{-1})$ and $\Delta z = O(Ha^{-1/2})$ between the side layer and the top at $y = f$ near $z = 1$, and (*e*) a corner region with $\Delta y = O(Ha^{-1})$ and $\Delta z = O(Ha^{-1})$ between the intersection region and the side at $y = f$ and $z = 1$. The slope of the top is discontinuous at $x = 0$, and there is an interior layer with $\Delta x = O(Ha^{-1/2})$ across the duct at this cross-section.

In the expansion for $x > 0$, u in the core is $O(Ha^{-1/2})$, and all the $O(1)$ flow for (3) is carried by a u of $O(Ha^{1/2})$ in the side layer. Walker *et al.* (1972) used Fourier transforms to reduce the expansion side-layer problem to an integro-differential equation and solved this equation with separation of variables. Their solution for the expansion side layer is correct.

Far upstream in the constant-area duct, the flow is fully developed with $u = a^{-1} + O(Ha^{-1/2})$ in the core and with a monotonic decrease of u to zero across the side layer. The key issue is how the $O(1)$ flow is transferred from the far upstream core to the side layer in the expansion at $x = 0^+$. Walker *et al.* (1972) indicated that there could be a u of $O(Ha^{1/2})$ inside the side layer in the constant-area duct, so that part of the $O(1)$ flow could enter the side layer upstream of the junction at $x = 0$. In their solution, the rest of the $O(1)$ flow enters the interior layer at $x = 0^-$ and is carried by a w of $O(Ha^{1/2})$ inside this layer to the side layer in the expansion.

For the side layer in the constant-area duct, the equations and boundary conditions presented by Walker *et al.* (1972) are correct, but are incomplete because they do not include any condition from matching the corner region at $y = a$ and $z = 1$. They stated, 'This problem cannot be solved using [Fourier] transforms because the solution contains singularities [at $y = a$ and $z = 1$] which are not acceptable to the transforms.' Using a superposition of the Green functions, they constructed a solution which satisfied their equations and boundary conditions. They acknowledged that their Green function solution is singular at the corner, but they did not investigate whether the corner-region solution could match the singularity in their side-layer solution. Cook, Ludford & Walker (1972) illustrated the critical role of the corner-region matching condition in a side-layer or interior-layer boundary value problem. Integrals of j_y at $y = a$ in the constant-area-duct side-layer solution of Walker *et al.* (1972) reveal that there is an $O(Ha^{-1/2})$ electric current between the side layer and corner region, i.e.

the singularity in their solution represents a source or sink of $O(Ha^{-1/2})$ electric current at the corner. With intersecting insulated walls, the corner region cannot provide or accept this current. When a corner-region matching condition excluding an electric current source or sink at the corner is added, the constant-area-duct side-layer problem of Walker *et al.* (1972) has only a zero solution, indicating that side layers with a u of $O(Ha^{1/2})$ are not possible in a constant-area duct. Therefore all the $O(1)$ flow and the $O(Ha^{-1/2})$ electric current must be transferred from the upstream core at $x = 0^-$ to the downstream side layer at $x = 0^+$ through the interior layer and through its intersection with the side layer with $\Delta x = O(Ha^{-1/2})$ and $\Delta z = O(Ha^{-1/2})$ at $x = 0$ and $z = 1$. Walker *et al.* (1972) did not treat the intersection of the side and interior layers, but they hypothesized that certain variables are continuous between the upstream and downstream side layers. Without a high-velocity side layer in the constant-area duct, these variables cannot be continuous and the intersection of the side and interior layers must be more complex than hypothesized by Walker *et al.* (1972).

Hunt & Ludford (1968) showed that an MHD flow with a strong transverse magnetic field and with insulated walls is constrained to follow certain characteristic surfaces. In the expansion of Walker *et al.* (1972), these surfaces are the cross-sections, forcing all the $O(1)$ flow into the side layer. In the constant-area duct, there are no characteristic surfaces, and the flow is relatively free. It is not surprising that the abrupt transition between a free flow and a highly constrained flow would be very complex, as it was in the solution of Hunt & Ludford (1968) for an obstacle in a constant-area duct. Here we avoid the difficulties of treating an abrupt transition because we only consider smooth expansions and contractions in which the slope and curvature of the top and bottom are continuous everywhere.

One alternative to the large-Hartmann-number asymptotic solution with the various subregions is a numerical solution of (1), (2) for an arbitrary value of Ha. Since we are interested in the range $Ha = 10^3$–10^5, any numerical scheme would need sufficient grid or collocation points inside the Hartmann layer, side layer and intersection region in order to resolve their large derivatives. Since the Hartmann layer and intersection region are much thinner than the side layer, their resolution would consume most of the computational resources. The Hartmann layer and intersection region involve a monotonic velocity variation which satisfies the no-slip condition at the top and which matches the tangential core or side-layer velocity. Therefore the arbitrary-Hartmann-number approach wastes most of the computational resources on the very uninteresting Hartmann layer and intersection region. Since the Hartmann layer and intersection region play a key role in the electric circuit, they cannot be ignored. Fortunately they both have the same simple, local, exponential structure (Moreau 1990).

In this paper we use the well-known analytical solution for the Hartmann layer and intersection region, and we devote all the computational resources to the core and side layer. This composite core-side-layer approach was developed by Ting *et al.* (1993), who treated the three-dimensional flow in a constant-area rectangular duct with thin electrically conducting walls and with a non-uniform transverse magnetic field. In terms of the asymptotic solution for $Ha \gg 1$, which involves asymptotic expansions in $Ha^{-1/2}$, the composite core–side-layer approach accurately combines the first two terms in both the core and side-layer asymptotic expansions into a single solution. The composite solution offers four advantages, namely: (i) there is no ambiguity about where the separate core and side-layer solutions apply for finite values of Ha, (ii) it indicates the presence or absence of a high-velocity side layer without *a priori* assumptions of orders, (iii) it includes the $O(Ha^{-1/2})$ core velocity so that it does not indicate that the core fluid is stagnant for any f' of $O(1)$ and (iv) it includes both

$O(Ha^{-1/2})$ and $O(Ha^{-1})$ electric currents and pressures, so that it includes the electric currents through the side and Hartmann layers and it includes both the $O(Ha^{-1/2})$ three-dimensional pressure drop and the $O(Ha^{-1})$ fully developed flow pressure gradient, as well as all other $O(Ha^{-1})$ pressure variations. We solve the composite core–side-layer problem with series of Chebyshev polynomials which automatically exclude singularities at the corner at $y = f$ and $z = 1$. Like the Fourier transform solutions of Walker *et al.* (1972) for the expansion side layer, our Chebyshev polynomial solutions automatically satisfy the corner-region matching condition.

We consider a smooth expansion between two different constant-area ducts, so that f' and f'' are continuous everywhere, and there are no interior layers. We drop the viscous term

$$Ha^{-2}(\partial^2 \boldsymbol{v}/\partial x^2 + \partial^2 \boldsymbol{v}/\partial y^2)$$

from (1), and we drop any term in an expression which is $O(Ha^{-1})$ smaller than another term in both the side layer and core. For example, we also drop $Ha^{-2}\,\partial^2 w/\partial z^2$ from the z-component of (1) because it is $O(Ha^{-1})$ while j_x is $O(1)$ in a high-velocity side layer, and it is $O(Ha^{-2})$ while j_x is $O(Ha^{-1/2})$ or $O(Ha^{-1})$ in a core region.

With simple manipulations, (1) become

$$u = \frac{\partial \phi}{\partial z} - \frac{\partial^2 \psi}{\partial x\,\partial y}, \quad v = \frac{\partial^2 \psi}{\partial x^2} + \frac{\partial^2 \psi}{\partial z^2}, \tag{4a, b}$$

$$w = -\frac{\partial \phi}{\partial x} - \frac{\partial^2 \psi}{\partial y\,\partial z}, \quad j_x = \frac{\partial^2 \psi}{\partial y\,\partial z}, \tag{4c, d}$$

$$j_y = -\frac{\partial \phi}{\partial y}, \quad j_z = -\frac{\partial^2 \psi}{\partial x\,\partial y} + Ha^{-2}\frac{\partial^3 \phi}{\partial z^3}, \tag{4e, f}$$

$$\frac{\partial^2 \phi}{\partial y^2} = Ha^{-2}\frac{\partial^4 \phi}{\partial z^4}, \quad \frac{\partial^2 \psi}{\partial y^2} = Ha^{-2}\frac{\partial^4 \psi}{\partial z^4}, \tag{4g, h}$$

where

$$\psi(x, y, z) = \int_0^y p(x, y^*, z)\,\mathrm{d}y^*. \tag{4i}$$

The terms $Ha^{-2}\,\partial^2 u/\partial z^2$, $Ha^{-2}\,\partial^3 p/\partial x\,\partial z^2$, and $Ha^{-2}\,\partial^4 \psi/\partial x^2\,\partial z^2$ have been dropped from (4*a*), (4*f*) and (4*h*), respectively. The problem has been reduced to two scalar functions governed by (4*g*, *h*). The boundary conditions at $z = 1$ are obtained by introducing (4*a*, *b*, *c*, *f*) into (2*c*, *d*) and no term is dropped.

The Hartmann-layer and intersection-region conditions at $y = f(x)$ require the right-handed orthogonal curvilinear coordinates n, s, z, where n is the distance from the top along the unit normal $\hat{\boldsymbol{n}}$ into the liquid metal and s is the distance along the top in the positive x-direction in any $z =$ constant plane. Walker *et al.* (1972) derived the conditions for a core or side layer from the local exponential Hartmann-layer and intersection-region solutions. For the present top with one degree of curvature, the conditions are

$$\boldsymbol{v}\cdot\hat{\boldsymbol{n}} = Ha^{-1}\left(\frac{\partial(\kappa v_s)}{\partial s} + \kappa\frac{\partial v_z}{\partial z}\right), \tag{5a}$$

$$\boldsymbol{j}\cdot\hat{\boldsymbol{n}} = Ha^{-1}\left(\frac{\partial v_s}{\partial z} - \frac{\partial v_z}{\partial s}\right), \tag{5b}$$

at $n = 0$, where $\kappa = -(\hat{\boldsymbol{n}}\cdot\hat{\boldsymbol{y}})^{-1}$. The right-hand side of (5*a*) is $O(Ha^{-1})$ smaller than the left-hand side for both the core and side layer, so that the composite core–side-layer

normal velocity is zero at the top. The right-hand side of (5*b*) is comparable to the left-hand side for both the core and side layer, reflecting the important role of the Hartmann layer in the electrical circuit. Introducing (4), (5) become

$$f'\left(\frac{\partial\phi}{\partial z}-\frac{\partial^2\psi}{\partial x\,\partial y}\right)=\frac{\partial^2\psi}{\partial x^2}+\frac{\partial^2\psi}{\partial z^2}, \tag{6a}$$

$$\frac{\partial^2\phi}{\partial x^2}+(1+(f')^2)\frac{\partial^2\phi}{\partial z^2}+f'\frac{\partial^2\phi}{\partial x\,\partial y}=Ha\left(\frac{\partial\phi}{\partial y}+f'\frac{\partial^2\psi}{\partial y\,\partial z}\right), \tag{6b}$$

at $y=f(x)$. The terms $\partial^3\psi/\partial y^2\,\partial z$ and $\partial^3\psi/\partial x\,\partial y\,\partial z$ have been dropped from (6*b*) because they are (Ha^{-1}) smaller than $Ha\,\partial^2\psi/\partial y\,\partial z$ in both the core and side layer. Neglecting the $O(Ha^{-1})$ volumetric flux deficiency in the Hartmann layer, the composite core–side-layer solution satisfies (3).

In this paper we only consider a smooth expansion between two constant-area ducts with $f=e_u$ for $x<-\hat{L}$, $f=e_d$ for $x>\hat{L}$ and

$$f=\tfrac{1}{2}(e_d+e_u)+\tfrac{1}{16}(e_d-e_u)\,X(15-10X^2+3X^4) \tag{7}$$

for $-\hat{L}<x<\hat{L}$, where $X=x/\hat{L}$. Here the origin lies at the centre of the expansion, while Walker *et al.* (1972) placed their origin at the junction of their constant-area duct and their expansion. In the next section, we present a general solution for the three-dimensional flow in a constant-area duct with a uniform magnetic field. In §4, this solution is used for $x<-\hat{L}$ and $x>\hat{L}$, and a numerical solution for the expansion for $-\hat{L}<x<\hat{L}$ completes the solution.

3. Three-dimensional flow in a constant-area duct

For the three-dimensional flow in a finite-length or semi-infinite duct with $f=e=$ a constant, we introduce the eigenfunction expansions

$$\phi=\phi_{fd}(y,z)+\sum_{n=1}^{\infty}C_n\,\phi_n(y,z)\exp(\lambda_n x), \tag{8a}$$

$$\psi=(C_0-Kx)\,y+\sum_{n=1}^{\infty}C_n\,\lambda_n^{-1}\,\psi_n(y,z)\exp(\lambda_n x), \tag{8b}$$

where ϕ_{fd} and K are the electric potential function and constant pressure gradient for fully developed flow. Equations (4*g*, *h*) are the governing equations for each pair of eigenfunctions ϕ_n, ψ_n and for ϕ_{fd}. With $f'=0$, (6) become

$$\lambda_n^2\,\psi_n+\frac{\partial^2\psi_n}{\partial z^2}=0,\quad \lambda_n^2\,\phi_n+\frac{\partial^2\phi_n}{\partial z^2}=Ha\frac{\partial\phi_n}{\partial y}, \tag{9a, b}$$

at $y=e$. Equations (2*c*, *d*) become

$$\frac{\partial\phi_n}{\partial z}=\frac{\partial\psi_n}{\partial y},\quad Ha^{-2}\frac{\partial^3\phi_n}{\partial z^3}=\frac{\partial\psi_n}{\partial y}, \tag{10a, b}$$

$$\lambda_n^2\,\psi_n+\frac{\partial^2\psi_n}{\partial z^2}=0,\quad \lambda_n^2\,\phi_n+\frac{\partial^2\psi_n}{\partial y\,\partial z}=0, \tag{10c, d}$$

at $z=1$. The boundary conditions for ϕ_{fd} are (9*b*) with $\lambda_n=0$ and (10*a*, *b*) with $\partial\psi_n/\partial_y$ replaced by $-K$. Each solution for $\lambda_n\neq 0$ automatically makes a zero contribution to (3), so that (3) determines K and scales ϕ_{fd}.

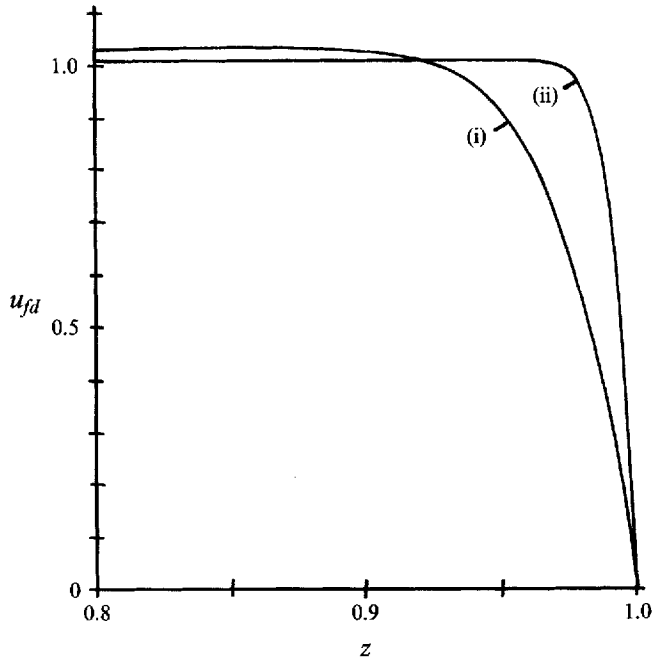

FIGURE 1. Axial velocity u_{fd} at $y = 0$ for fully developed flow in a square duct ($e = 1$) for: (i) $Ha = 10^3$ and (ii) $Ha = 10^4$.

For a Chebyshev spectral collocation solution (Canuto *et al.* 1988), we introduce the series

$$\phi_n = \sum_{l=0}^{NY} \sum_{m=0}^{NZ} A_{lm}^{(n)} T_{2l}(Y) T_{(2m+1)}(z), \tag{11a}$$

$$\psi_n = \sum_{l=0}^{(NY-1)} \sum_{m=0}^{(NZ+1)} B_{lm}^{(n)} T_{(2l+1)}(Y) T_{2m}(z), \tag{11b}$$

where $Y = y/e$ and $T_n(x) = \cos[n \arccos(x)]$ are the Chebyshev polynomials. Equation (11*a*) is also used for ϕ_{fd}. The collocation points are $Y_j = \cos(j\pi/2NY)$, $z_k = \cos(k\pi/2NZ)$. Equations ($4g, h$) are applied at the interior collocation points. Since ($4g, h$) do not involve λ_n, we solve the resultant algebraic equations for $(2NY \times NZ - NY - NZ)$ of the unknown coefficients in terms of the remaining $(4NY + 2NZ + 1)$ coefficients for $l = 0$ or $m = 0$ and 1. Equations (9) are applied at the collocation points z_k at $y = e$, and (10) are applied at the collocation points Y_j at $z = 1$. Introducing the solution for ($4g, h$), we obtain a relatively small matrix whose determinant gives the characteristic equation for λ_n^2. For each λ_n, $A_{lm}^{(n)}$ and $B_{lm}^{(n)}$ are determined with the normalization that each mode's axial velocity is -1 at $y = z = 0$, because we expect three-dimensional effects to reduce u at $y = z = 0$ from its fully developed value. Equation (3) scales $A_{lm}^{(fd)}$ and determines K.

Since there is no need to resolve the Hartmann layer, small values of NY are sufficient. All the results in this paper were the same for $NY = 4$, 5 and 6. Since the side layer is resolved, NZ must be larger and must be increased as Ha is increased. Fortunately the collocation points z_k are concentrated near $z = 1$. For all results to be independent of NZ, we needed $NZ = 24$ for $Ha = 10^4$ and $NZ = 30$ for $Ha = 10^5$.

The axial velocity at $y = 0$ for fully developed flow for $e = 1$ and $Ha = 10^3$ and 10^4 is plotted in figure 1. For $Ha \geqslant 10^3$ and all values of e, the values of K agree very well

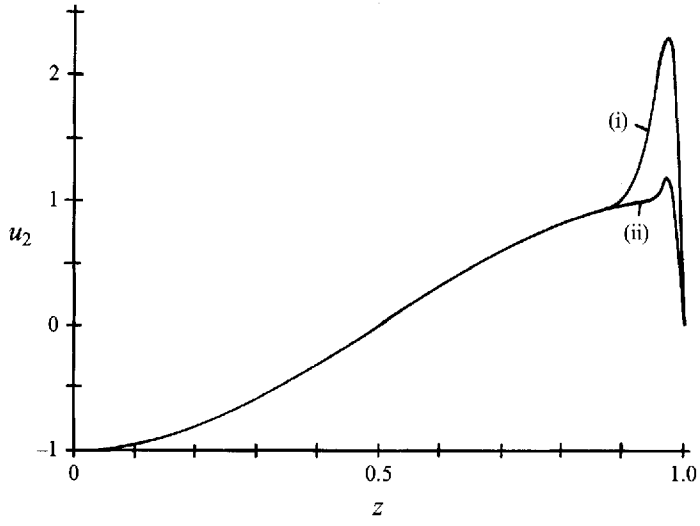

FIGURE 2. Axial velocity u_2 at $y = 0$ for the second eigenvalue, for $e = 1$ and for: (i) $Ha = 10^3$ and (ii) $Ha = 10^4$.

with the values computed from the $O(Ha^{-1})$ and $O(Ha^{-3/2})$ terms in the large-Ha asymptotic solution for the fully developed flow pressure gradient (Roberts 1967).

None of the eigenfunctions involve a high-velocity side layer. Certain eigenfunctions have an $O(1)$ velocity overshoot inside the side layer, but these overshoots all decrease as Ha is increased. For the second eigenvalue for $e = 1$, $u_2(0, z)$ is plotted in figure 2 for $Ha = 10^3$ and 10^4. For $Ha = 10^5$, the side layer for every eigenvalue has a monotonic variation of u from 0 at $z = 1$ to the core value.

The numerical results indicate that the eigenvalues can be grouped into three families. For two of these families, the values of λ_n have very weak variations with e, and these variations become even weaker as Ha is increased. For large Ha, the eigenfunctions in these two families are independent of y (or linear in y for ψ_n). The characteristics of these two families for $Ha \gg 1$ are easily derived from the problem (4g, h), (9), (10) with $\partial\phi_n/\partial y = \partial^2\psi_n/\partial y^2 = 0$, and these characteristics agree very well with the numerical results for $Ha = 10^3$, 10^4 or 10^5.

For $Ha \gg 1$, and for the first family of eigenvalues, $\lambda_n = (k+0.5)\pi + O(Ha^{-2})$, for $k = 0, 1, 2, \ldots$, and for any e. The core solutions for this family for $Ha \gg 1$ are

$$\phi_n = \frac{2Ha}{e\lambda_n^3}\sin(\lambda_n z) - z\cos(\lambda_n z), \quad p_n = \frac{2Ha}{e\lambda_n^3}\cos(\lambda_n z),$$

$$u_n = \lambda_n z\sin(\lambda_n z) - \cos(\lambda_n z), \quad w_n = \lambda_n z\cos(\lambda_n z),$$

$$j_{xn} = -\frac{2Ha}{e\lambda_n^2}\sin(\lambda_n z), \quad j_{zn} = -\frac{2Ha}{e\lambda_n^2}\cos(\lambda_n z),$$

while $v_n = O(Ha^{-1})$ and $j_{yn} = O(Ha^{-2})$. Since j_{xn} and j_{zn} are $O(Ha)$ larger than u_n and w_n, these are electric-current modes – when they complete the circuit for the $O(Ha^{-1/2})$ three-dimensional electric current, the associated fluid velocity is $O(Ha^{-3/2})$.

For $Ha \gg 1$ and for the second family of eigenvalues, $\lambda_n = k\pi + O(Ha^{-1/2})$ for $k = 1, 2, \ldots$, and for any e. These eigenvalues approach their large-Ha values more gradually than the first family. For example for arbitrary values of Ha and for $e = 1$,

λ_n is 10.133, 9.557 and 9.458 for $Ha = 10^3$, 10^4 and 10^5, respectively, while $3\pi = 9.425$. The weak variations with e vanish as Ha is increased. The core solutions for this family for $Ha \gg 1$ are

$$u_n = -\cos(\lambda_n z), \quad w_n = \sin(\lambda_n z), \quad \phi_n = -\lambda_n^{-1} \sin(\lambda_n z),$$

while j_{xn}, j_{zn} and p_n are $O(Ha^{-1/2})$. The cosine variation of u for $k = 1$ is evident in figure 2. These modes play a role in the redistribution of both flow and electric current since the $O(1)$ flow is tied to the $O(Ha^{-1/2})$ electric current.

The numerical determination of the values of λ_n for arbitrary values of Ha and any e yields a list of eigenvalues. The eigenvalues that are converging to either $(k+0.5)\pi$ or $k\pi$ as Ha is increased are easily identified. The remaining eigenvalues for an arbitrary Ha are the members of the third family. The λ_n in the third family vary as e is changed, and the eigenfunctions involve variations with y, even for large values of Ha. For $Ha = 10^3$, the first eigenvalue in this family is 3.359, 1.630 and 1.088 for $e = 1$, 2 and 3, respectively. The eigenfunctions have the same orders as the second family, i.e. u_n, w_n and ϕ_n are $O(1)$, while j_{xn}, j_{zn} and p_n are $O(Ha^{-1/2})$.

Many problems involve two semi-infinite, constant-area ducts with uniform magnetic fields, which are separated by a source of a three-dimensional disturbance, such as an expansion, a non-uniform magnetic field region or a manifold. In all such problems, the present eigenfunction solutions can be used in the constant-area ducts with the coefficients C_n for each constant-area duct determined by matching the numerical solution for the finite-length disturbance region. The advantage over extending the numerical solution far upstream and downstream in the constant-area ducts is that the eigenfunction solutions involve only a few unknowns. Obviously the eigenvalues occur in pairs, $\pm\lambda_n$. In the next section the positive and negative values are used for $-\infty < x < -\hat{L}$ and $\hat{L} < x < \infty$, respectively. For a finite-length duct with three-dimensional disturbances at both ends, both positive and negative eigenvalues would be kept.

4. Solution for a smooth expansion

For $x < -\hat{L}$ or for $x > \hat{L}$, we use (8) with the K, ϕ_{fd}, positive or negative λ_n, ϕ_n and ψ_n for Ha and $e = e_u$ or $e = e_d$. The pressure level is fixed by setting $C_0 = 0$ in the downstream solution, i.e. so that the pressure far downstream is $-K_d x$. For the expansion for $-\hat{L} < x < \hat{L}$, we introduce $Y = y/f(x)$. This has little effect on (4g, h), but (2c, d) and (6) are changed. Paralleling (11), we introduce the series

$$\phi = \sum_{n=0}^{NX} \sum_{l=0}^{NY} \sum_{m=0}^{NZ} A_{nlm}\, T_n(X)\, T_{2l}(Y)\, T_{(2m+1)}(z), \tag{12a}$$

$$\psi = \sum_{n=0}^{NX} \sum_{l=0}^{(NY-1)} \sum_{m=0}^{(NZ+1)} B_{nlm}\, T_n(X)\, T_{(2l+1)}(Y)\, T_{2m}(z). \tag{12b}$$

The axial collocation points are $X_i = \cos(i\pi/NX)$. Equations (4g, h) are applied at the interior collocation points, (6) are applied at the collocation points on the top at $Y = 1$ and (2c, d) are applied at the collocation points on the side at $z = 1$. At $x = \pm\hat{L}$, ϕ, ψ, $\partial\phi/\partial x$ and $\partial\psi/\partial x$ must be continuous. Continuity of ϕ and ψ is applied at every collocation point at $x = \pm\hat{L}$. Since $f'(\pm\hat{L}) = f''(\pm\hat{L}) = 0$, the equations show that continuity of $\partial\phi/\partial x$ and $\partial\psi/\partial x$ along the lines at $x = -\hat{L}$, $y = e_u$ and at $x = \hat{L}$, $y = e_d$ is sufficient to guarantee their continuity over the rest of these cross-sections. The number of collocation points along the lines at $x = -\hat{L}$, $y = e_u$ and at $x = \hat{L}$, $y = e_d$

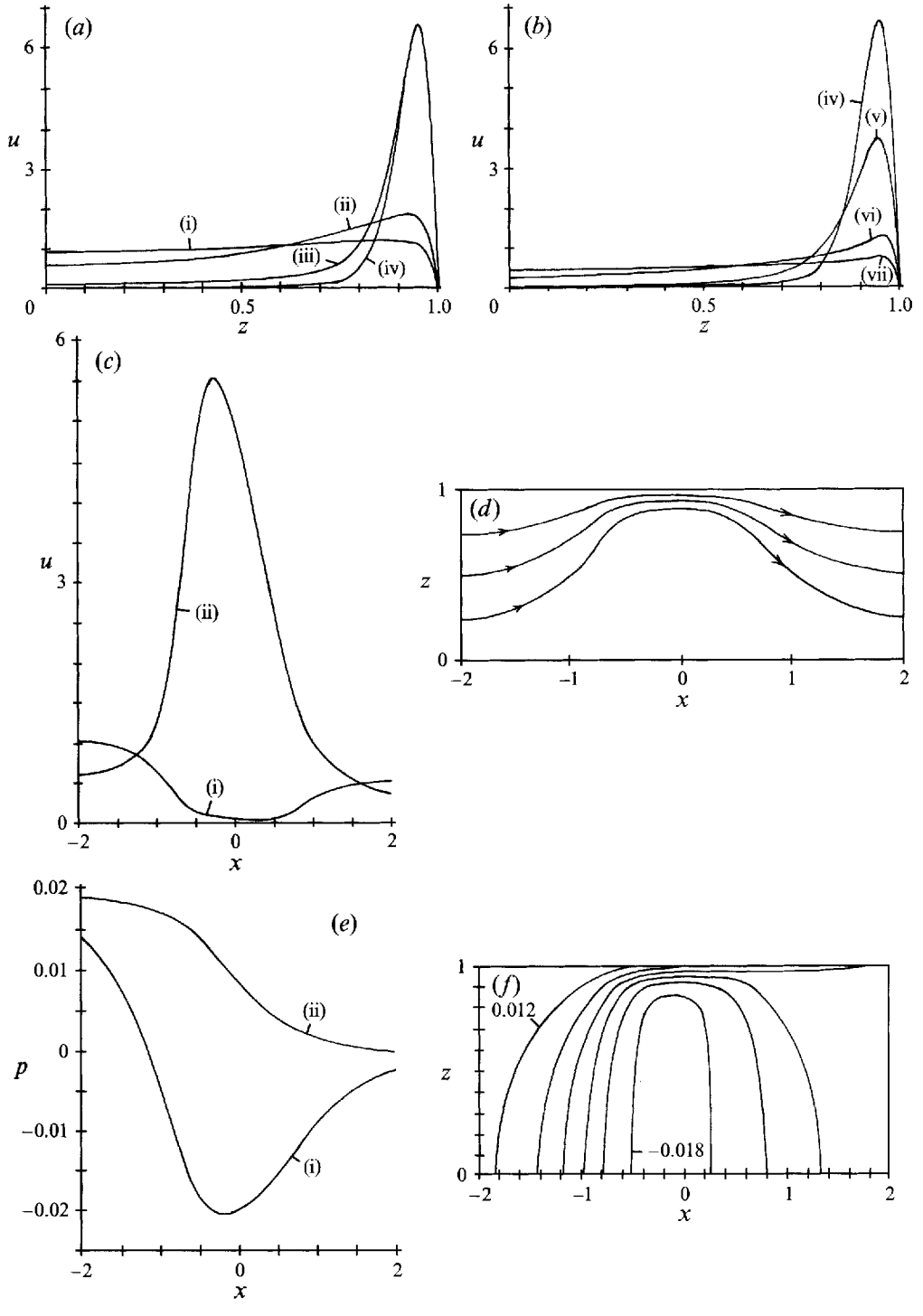

FIGURE 3. Results for $Ha = 10^3$, $e_u = 1$, $e_a = 2$ and $\hat{L} = 1$. (*a*, *b*) Axial velocity u at $y = 0$ *vs.* z: (i) $x = -1.5$, (ii) $x = -1.0$, (iii) $x = -0.5$, (iv) $x = 0$, (v) $x = 0.5$, (vi) $x = 1.0$ and (vii) $x = 1.5$. (*c*) Axial velocity u at $y = 0$ *vs.* x: (i) $z = 0$ and (ii) $z = 0.98$. (*d*) Rough sketch of streamlines for the integrals of u and w from $y = 0$ to $y = f(x)$. (*e*) Pressure p at $y = 0$ *vs.* x: (i) $z = 0$ and (ii) $z = 1.0$. (*f*) Contours of constant pressure in the $y = 0$ plane.

determines where the series (8) are truncated. The downstream-duct series are truncated at $n = (2NZ-1)$, but the upstream-duct series are truncated at $n = (2NZ-2)$ because (8) still includes the constant pressure C_0 to be determined. We used $NX = 24$ for every case presented here. A smaller value of NX would probably have given equally good results but we did not explore this possibility because the code required so little time. Each case required less than 20 minutes on a Convex C3880 supercomputer using four parallel processors.

For every case presented here, $e_u = 1$, i.e. a square upstream duct. The remaining parameters are Ha, e_d and $\hat{L}$. We consider variations from a base case with $Ha = 10^3$, $e_d = 2$ and $\hat{L} = 1$. The base-case results are presented in figure 3. In the upstream constant-area duct, the flow migrates towards $z = 1$. At $x = -\hat{L}$, u is 0.62 and 1.7 at $z = 0$ and $z = 0.96$. At $x = -0.5$ and $x = 0$, there is a strong side-layer jet with a maximum value of u of 6.6 or $0.21Ha^{1/2}$. There is some residual flow in the core, but it is very small at $x = 0$. As x increases from zero, the flow migrates out of the side layer and into the core. At $x = \hat{L}$, there is a modest flow concentration near $z = 1$ which decays in the downstream constant-area duct. Along the centreline at $y = z = 0$, u reaches a minimum of 0.018 or $0.57Ha^{-1/2}$ at $x = 0.3$. The velocity at $z = 0.98$ is between the peak side-layer velocity and the side for this Ha, but the curve in figure 3(*c*) still illustrates the growth and decay of the side-layer jet in the expansion. The maximum side-layer velocity occurs upstream of the minimum core velocity because the cross-sectional area is increasing.

Since the flow is three-dimensional, there is no stream function, but there is a stream function for the integrals of u and w from $y = 0$ to $y = f(x)$. A rough sketch of the streamlines for these integrals of u and w is presented in figure 3(*d*). In the upstream constant-area duct the flow migrates towards $z = 1$. As x increases from -1, the flow migrates into the side layer where it is concentrated for roughly $-0.5 < x < 0.5$. The return to the downstream fully developed flow is similar to the upstream departure from its fully developed flow. Walker *et al.* (1972) treated an abrupt change in slope where the flow was transferred from the core to the side layer inside an interior layer at the cross-section of the junction. With the present smooth geometry, their interior layers are spread over the regions of the expansion for roughly $0.5 < |x| < 1.0$, where the slope gradually changes from zero to an $O(1)$ value. Virtually all the required vertical redistribution of the flow occurs in the expansion, especially near $x = 0$.

For $e_u = 1$ and $e_d = 2$, the values of ϕ at $z = \pm 1$ are roughly ± 1 and ± 0.5 in the upstream and downstream fully developed flows, respectively. The associated axial voltage differences drive axial electric currents in the positive and negative x-directions for $z > 0$ and $z < 0$, respectively. Since there are no axial currents in fully developed flow, the circuit for the axial currents must be completed by positive and negative values of j_z upstream and downstream, respectively. Equations (4*d*, *i*) indicate that the integral of j_x from $z = 0$ to $z = 1$ equals the pressure difference between $z = 0$ and $z = 1$. The vertical distance between the two curves in figure 3(*e*) is proportional to the axial electric current at each cross-section. Therefore the axial electric current is maximum near $x = 0$, and there are still some axial currents at $x = \pm 2$. Walker *et al.* (1972) showed that for $f' = O(1)$, the axial electric current is confined to the side layer, while $j_x = O(Ha^{-3/2})$ in the core. Since the thin side layers have a large electrical resistance, the $O(1)$ axial voltage differences only drive an $O(Ha^{-1/2})$ axial electric current inside the side layers, but this current is still large compared to the $O(Ha^{-1})$ fully developed flow current. The current in the positive z-direction upstream creates a large pressure drop along the centreline. When the same current flows in the negative z-direction downstream, it creates a pressure rise along the centreline. Since the

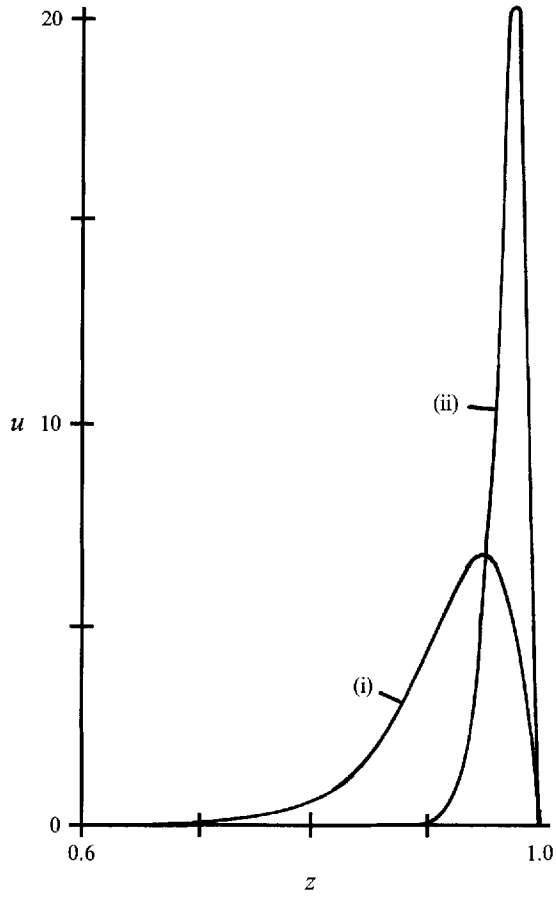

FIGURE 4. Axial velocity u at $x = y = 0$ for $e_u = 1$, $e_d = 2$ and $\hat{L} = 1$: (i) $Ha = 10^3$ and (ii) $Ha = 10^4$.

transverse current is spread over a larger Δy downstream, the downstream pressure rise is smaller than the upstream pressure drop, so that the three-dimensional electric current circulation produces a net pressure drop Δp_{3D}. The same net pressure drop occurs at the side, but here it is due to the much larger viscous shear stresses associated with the $O(Ha^{1/2})$ velocities in the side layer. The larger pressure gradient at the side wall of the expansion is evident in figure 3(*e*). We define Δp_{3D} relative to a reference pressure variation, namely $p = -K_u x$ for $x < 0$ and $p = -K_d x$ for $x > 0$, where K_u and K_d are the pressure gradients K for the fully developed flows in the upstream and downstream constant-area ducts. The values of K_u and K_d used in the reference pressure are the values determined in the numerical solutions for the constant-area ducts. As $x \to \infty$, the actual and reference pressures approach the same straight line with slope K_d, but as $x \to -\infty$, the actual and reference pressures approach two parallel straight lines, both with slope K_u and with the actual pressure greater than the reference pressure by Δp_{3D}. For $-\hat{L} < x < \hat{L}$, the reference pressure drop is larger than that for locally fully developed flow at each cross-section of the expansion, but the locally fully developed pressure variation is not a good reference because its evaluation would require a numerical integration of the fully developed pressure gradient for each $f(x)$. For $Ha = 10^3$ and $e_d = 2$, the reference pressure drop is larger than the locally fully developed drop by $1.663 \times 10^{-4}\hat{L}$. For the base case, $\Delta p_{3D} = 1.682 \times 10^{-2}$.

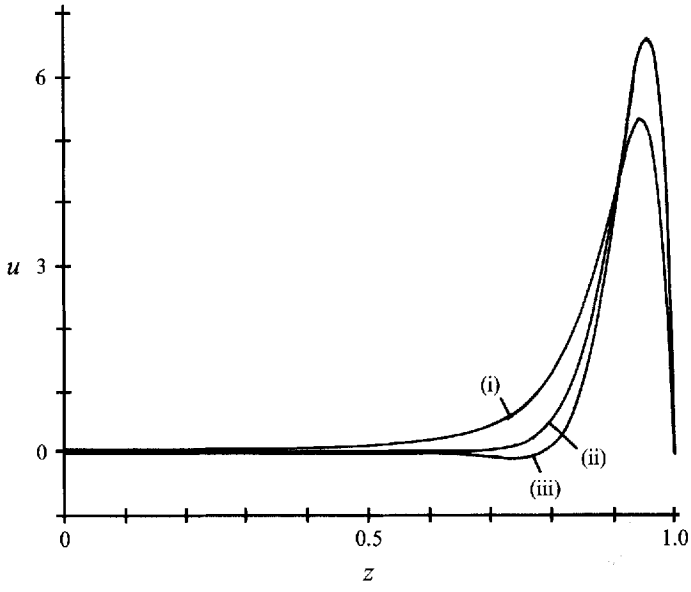

FIGURE 5. Axial velocity u at $x = y = 0$ for $Ha = 10^3$, $e_u = 1$ and $\hat{L} = 1$: (i) $e_d = 1.5$, (ii) $e_d = 2.0$ and (iii) $e_d = 3.0$.

The contours of constant pressure in the $y = 0$ plane for the base case are presented in figure 3(f). The expansion occupies $-1 < x < 1$. In the core, these isobars are the streamlines for j_x and j_z because the last term in (4f) is negligible. Inside the side layer, the transverse current j_z is turned by the insulated side to flow upward to the intersection region at $y = f$. In (4f) $Ha^{-2}\partial^3\phi/\partial z^3$ cancels $\partial p/\partial x$ at $z = 1$, so that j_z is zero at the side. The isobars in figure 3(f) illustrate the three-dimensional circulation of electric current driven by the axial voltage differences. The concentration of axial electric current in the side layer is evident near $x = 0$ where the slope f' is maximum. Far upstream and downstream, the isobars would be vertical lines in figure 3(f).

For $e_d = 2$ and $\hat{L} = 1$, we obtained results for $Ha = 10^3$, 5×10^3, 10^4, 5×10^4 and 10^5. The formula

$$\Delta p_{3D} = 0.6168 Ha^{-1/2} - 2.68 Ha^{-1}$$

gives values which fit the results for all five cases. The axial pressure variations for all five cases look like the curves in figure 3(e), except that the magnitudes of all pressures decrease as Ha is increased. The distance upstream and downstream of the expansion required to complete the circuit for the three-dimensional electric current and to achieve fully developed flow is roughly $\Delta x = 2$ for every case. The maximum side-layer velocity at $x = -0.3$ is 23 or $0.23 Ha^{1/2}$ for $Ha = 10^4$ and 75.9 or $0.24 Ha^{1/2}$ for $Ha = 10^5$. The axial velocities at $x = y = 0$ for $Ha = 10^3$ and 10^4 are plotted in figure 4. The minimum centreline velocity occurs at $x = 0.3$ for all five cases and decreases as Ha is increased until $u_{min} = 0.002$ for $Ha = 10^5$.

For $Ha = 10^3$ and $\hat{L} = 1$, $100\Delta p_{3D}$ is 0.9545, 1.682 and 2.453 for $e_d = 1.5$, 2 and 3, respectively. Since the downstream values of ϕ at $z = \pm 1$ are roughly $\pm 1/e_d$, the three-dimensional electric current circulation and Δp_{3D} increase as e_d is increased. Again the axial pressure variations look like the curves in figure 3(e), but the slope of p at $z = 1$ in the expansion increases as e_d is increased. For $Ha = 10^3$ and $\hat{L} = 1$, the minimum centreline velocity is 0.070, 0.018 and -0.0054 for $e_d = 1.5$, 2 and 3, respectively. For

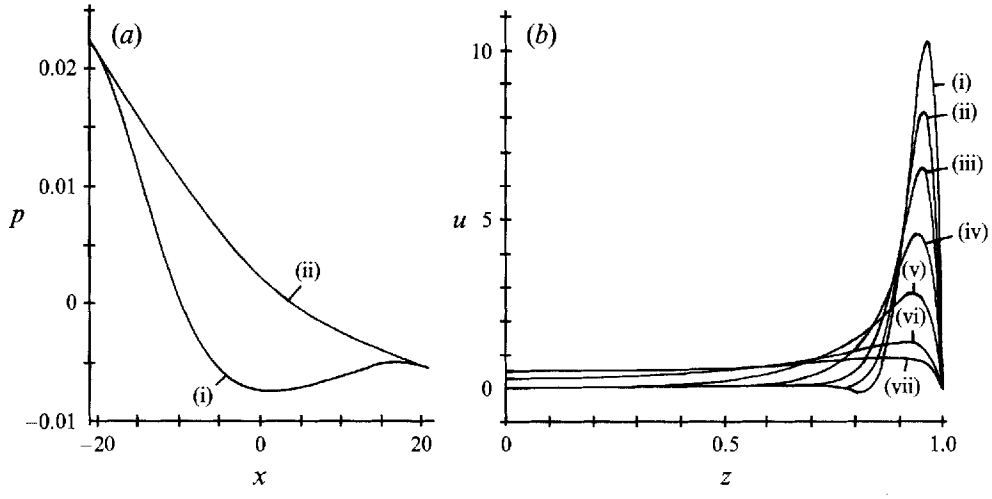

FIGURE 6. Results for $Ha = 10^3$, $e_u = 1$ and $e_d = 2$. (*a*) Pressure p at $y = 0$ for $\hat{L} = 20$: (i) $z = 0$ and (ii) $z = 1.0$. (*b*) Axial velocity u at $x = y = 0$ for: (i) $\hat{L} = 0.25$, (ii) $\hat{L} = 0.5$, (iii) $\hat{L} = 1.0$, (iv) $\hat{L} = 2.0$, (v) $\hat{L} = 4.0$, (vi) $\hat{L} = 10.0$ and (vii) $\hat{L} = 20.0$.

$e_d = 3$, there is a small recirculating flow near $x = 0$. The axial velocities at $x = y = 0$ for $e_d = 1.5$, 2 and 3 are plotted in figure 5. For $e_d = 3$, there is a velocity dip just outside the side layer, so that the largest negative velocity is $u = -0.2$ at $z = 0.75$.

For $Ha = 10^3$ and $e_d = 2$, $100\Delta p_{3D}$ is 2.120, 1.938, 1.682, 1.399, 1.088, 0.5552 and 0.0816 for $\hat{L} = 0.25$, 0.5, 1, 2, 4, 10 and 20, respectively. In the expansion, the axial electric current is confined to the side layer. When $\hat{L}$ is small, the short expansion represents a smaller resistance to the axial voltage difference, and the three-dimensional electric current circulation is larger. As $\hat{L}$ becomes large, the flow should become locally fully developed, but Walker & Ludford (1972) showed that this requires $\hat{L} \gg Ha^{1/2}$. For $\hat{L} = O(Ha^{1/2})$ the current and flow from the side layer are spread over the entire cross-section, but there are still significant three-dimensional effects. The axial pressure variations plotted in figure 6(*a*) illustrate that there is still a pressure difference between $z = 0$ and $z = 1$ due to axial currents for $\hat{L} = 20 = 0.63Ha^{1/2}$. The axial velocity at $x = y = 0$ is plotted in figure 6(*b*) for the seven values of $\hat{L}$. For $\hat{L} = 0.25$ and 0.5, there is reverse flow just outside the side-layer jet. In the expansion the maximum slope is $15(e_d - e_u)/16\hat{L}$ at $x = 0$ so that increasing $(e_d - e_u)$ or decreasing $\hat{L}$ increases the slope and a large slope leads to reverse flow. For $\hat{L} = 20$, the velocity is essentially that for locally fully developed flow, even though the pressure and electric current are not.

5. Conclusions

We have presented a method to treat three-dimensional liquid-metal flows in electrically insulated ducts with rectangular cross-sections and with strong transverse magnetic fields. The eigenfunction solutions can be used for many different problems involving a three-dimensional disturbance between two constant-area ducts. We have shown that side layers with large $O(Ha^{1/2})$ velocities do not occur in constant-area ducts, although the core flow often becomes concentrated near the sides. We have applied our method to a smooth expansion between two different constant-area ducts. High-velocity side layers do occur in the expansion, and the core velocity near the

cross-section with maximum slope is often very small or negative for strong three-dimensional effects, i.e. large aspect ratio differences between the two ducts or short expansions with large slope. In many technological applications the objective is to minimize the overall pressure drop, based on the small $O(Ha^{-1})$ pressure gradient for the fully developed flow in an electrically insulated duct. However, the $O(Ha^{-1/2})$ pressure drops associated with three-dimensional current circulations at expansions, contractions, non-uniform magnetic field regions, elbows, manifolds, etc., may make major contributions to the overall pressure drop. Extremely gradual transitions over dimensionless lengths which are much greater than $Ha^{1/2}$ are required to avoid three-dimensional pressure drops and to achieve locally fully developed flow.

There is only a minor difference between the present solution and that presented by Walker *et al.* (1972). In both solutions, the flow for $z > 0$ in each constant-area duct near its junction with the expansion is concentrated near the side at $z = 1$. In the solution of Walker *et al.* (1972), this flow concentration is split between an $O(Ha^{1/2})$ velocity in the side layer and a large, but $O(1)$ velocity in the core near $z = 1$. In the present corrected solution, there is no $O(Ha^{1/2})$ velocity in the constant-area-duct side layer, so that the flow concentration in either constant-area duct involves only a large $O(1)$ core velocity near $z = 1$.

The present flow is essentially what one would expect from the characteristic-surface concept of Hunt & Ludford (1968). The relatively free flow in a constant-area duct and in the part of the expansion where $f' \ll Ha^{-1/2}$ responds to the three-dimensional effects by moving towards the side. The flow in the expansion where $f' \gg Ha^{-1/2}$ is blocked by the characteristic surfaces and is concentrated as an $O(Ha^{1/2})$ velocity in the side layer. In figures 3(*a*) and 3(*b*), u at $x = \pm 0.5$ and at $x = 0$ has a high-velocity side layer and only an $O(Ha^{-1/2})$ residual velocity in the core.

The relationship between f' and $Ha^{-1/2}$ is best illustrated by the velocity profiles in figure 6(*b*). For curves (i)–(vii), $f'Ha^{1/2}$ is 118.6, 59.3, 29.7, 14.8, 7.4, 3.0 and 1.5, respectively. For $f'Ha^{1/2} > 7$, there is a distinct side layer and a very small core velocity, although the side layer occupies $0.4 < z < 1$ for $f'Ha^{1/2} = 7.4$. For $f'Ha^{1/2} = 3$, there is only a core with slight flow concentration near $z = 1$. For $f'Ha^{1/2} = 1.5$, the velocity is essentially that for locally fully developed flow. Therefore the present results quantify the relationship between the wall slope and Hartmann number for blocked and free flows.

This research was supported by the McDonnell Douglas Aerospace Corporation as part of the International Thermonuclear Experimental Reactor (ITER) Design Project. This research was also supported by the US National Science Foundation under Grants CTS 94-19484 and CTS 95-0016N. The calculations were performed on a Convex C3880 supercomputer at the National Center for Supercomputer Applications at the University of Illinois at Urbana-Champaign.

REFERENCES

CANUTO, C., HUSSAINI, M. Y., QUARTERONI, A. & ZANG, T. A. 1988 *Spectral Methods in Fluid Dynamics*. Springer.

COOK, L. P., LUDFORD, G. S. S. & WALKER, J. S. 1972 Corner regions in the asymptotic solution of $\epsilon\nabla^2 u = \partial u/\partial y$ with reference to MHD duct flow. *Proc. Camb. Phil. Soc.* **72**, 117–122.

HUNT, J. C. R. & LUDFORD, G. S. S. 1968 Three-dimensional MHD duct flows with strong transverse magnetic fields. Part 1. Obstacles in a constant-area channel. *J. Fluid Mech.* **33**, 693–714.

MOREAU, R. 1990 *Magnetohydrodynamics*. Kluwer.

ROBERTS, P. H. 1967 *An Introduction to Magnetohydrodynamics.* Elsevier.

TING, A., HUA, T. Q., WALKER, J. S. & PICOLOGLOU, B. F. 1993 Liquid-metal flow in a rectangular duct with thin metal walls and with a non-uniform magnetic field. *Intl J. Engng Sci.* **31**, 357–372.

WALKER, J. S. & LUDFORD, G. S. S. 1972 Three-dimensional MHD duct flows with strong transverse magnetic fields. Part 4. Fully insulated, variable-area rectangular ducts with small divergences. *J. Fluid Mech.* **56**, 481–496.

WALKER, J. S., LUDFORD, G. S. S. & HUNT, J. C. R. 1972 Three-dimensional MHD duct flows with strong transverse magnetic fields. Part 3. Variable-area rectangular ducts with insulating walls. *J. Fluid Mech.* **56**, 121–141.